Thermospheric Temperature and Density Variability During 3 to 4 February 2022 Minor Geomagnetic Storm: The SpaceX Satellite Loss Event

F. I. Laskar[1], E. K. Sutton[2], D. Lin[3], K. R. Greer[1], S. Aryal[1], X. Cai[1], N. M. Pedatella[3], R. W. Eastes[1], W. Wang[3], M. V. Codrescu[4], W. E. McClintock[1]

[1]Laboratory for Atmospheric and Space Physics, University of Colorado, Boulder, CO, USA
[2]Space Weather Technology, Research, and Education Center (SWx TREC), University of Colorado at Boulder, CO, USA
[3]High Altitude Observatory, National Center for Atmospheric Research, Boulder, CO, USA
[4]Space Weather Prediction Center, NOAA, Boulder, CO, USA

Key Points:

- GOLD observed a ∼60 K rise in lower-to-middle thermospheric temperature during a minor geomagnetic storm on 3 to 4 February 2022
- GOLD-informed MSIS calculations indicate an increase in density by 15% (at 150 km) to 80% (500 km)
- MAGE temperature and neutral density enhancements due the storm are in good agreement with GOLD-informed MSIS.

Corresponding author: Fazlul I. Laskar, Fazlul.Laskar@colorado.edu

Abstract

Themospheric conditions during a minor geomagnetic event of 3 and 4 February 2022 has been investigated using disk temperature (T_{disk}) observations from Global-scale Observations of the Limb and Disk (GOLD) mission and model simulations. GOLD observed that the T_{disk} increases by more than 60 K during the storm event when compared with pre-storm quiet days. A comparison of the T_{disk} with effective temperatures (i.e., a weighted average based on airglow emission layer) from Mass Spectrometer Incoherent Scatter radar version 2 (MSIS2) and Multiscale Atmosphere-Geospace Environment (MAGE) models shows that MAGE outperforms MSIS2 during this particular event. MAGE underestimates the T_{eff} by about 2%, whereas MSIS2 underestimates it by 7%. As temperature enhancements lead to an expansion of the thermosphere and resulting density changes, the value of the temperature enhancement observed by GOLD can be utilized to find a GOLD equivalent MSIS2 (GOLD-MSIS) simulation – from a set of MSIS2 runs obtained by varying geomagnetic ap index values. From the MSIS2 runs we find that an ap value of 116 nT produces a T_{eff} perturbation that matches with the GOLD T_{disk} enhancement. Note that during this storm the highest value of the 3 hr cadence ap was 56 nT. From the MSIS-GOLD run we found that the thermospheric density enhancement varies with altitude from 15% (at 150 km) to 80% (at 500 km). Independent simulations from the MAGE model also show a comparable enhancement in neutral density. These results suggest that even a modest storm could impact the thermospheric densities significantly.

Plain Language Summary

The background variation of the thermosphere-ionosphere (TI) system is mainly controlled by solar radiation and the perturbations in the TI system are primarily governed by solar transient events, such as, solar flares and coronal mass ejections. Lower atmospheric waves also influence the TI system significantly. The majority of the transient energy transport from the solar wind to the TI system occurs through high latitude. Such energy deposition can result in significant density increase in the TI system that increases the drag for low and very-low earth orbiting satellites which can result in deorbiting. A famous example of such is the loss of 38 satellites by SpaceX on 3 February 2022, which they attributed to a modest geomagnetic storm, the economic value of which is thought to be several tens of millions of dollars. In this work we have investigated the neutral properties of this geomagnetic event and provided experimental and

simulation results on the quantification of thermospheric temperature and density variability.

1 Introduction

The Thermosphere-Ionosphere (TI) system of the Earth is externally forced by waves from the lower atmosphere and energy and momentum inputs from the sun. The thermospheric background neutral density and temperature are controlled directly by solar irradiance, one form of solar forcing. Another form of solar forcing comes from solar wind particles interacting with Earth's magnetic field and depositing energy into the TI system to generate perturbations. Perturbations can also be generated by waves propagating upwards from the lower atmosphere and by solar transient events like solar flares. These perturbations in thermospheric temperature and neutral density can disrupt the ionospheric communications and satellite-based navigation. With the rise of private sector space exploration industries that are launching thousands of satellites, it is crucial to understand the physical processes and to improve forecast of the TI system.

The solar wind particles entering into the TI at high latitudes create enhanced temperatures through Joule heating, which eventually enhances the global temperature (Laskar, Eastes, et al., 2021; Richmond, 2021). The enhanced temperature leads to thermospheric density increase at a given altitude (e.g., Fuller-Rowell et al., 1994; Prölss, 2010; Richmond, 2021). The resultant enhanced density leads to larger satellite drag, particularly for the Low-Earth-Orbit (LEO) satellites (Sutton et al., 2005; Li & Lei, 2021). Most of the earlier studies have concentrated on the impact of major storms on the thermosphere (e.g., H. Liu & Lühr, 2005; Sutton et al., 2005; Bruinsma et al., 2006; R. Liu et al., 2010; Yuan et al., 2019). But in recent times, with the availability of synoptic and rich local time data from geostationary satellites, it has been observed that even minor storms (with ap index less than 14 nT) can also impact the thermosphere significantly (Laskar, Eastes, et al., 2021; Cai, Burns, Wang, Qian, Pedatella, et al., 2021; Cai, Burns, Wang, Qian, Solomon, et al., 2021; Aa et al., 2021). An example of the consequences of such increases in satellite drag during a modest storm is the loss of 38 out of 49 satellites during the 38^{th} launch of the SpaceX's Starlink constellation (Hapgood et al., 2022). The impact of these minor storms are not well represented in physics based general circulation models (Cai, Burns, Wang, Qian, Pedatella, et al., 2021). Therefore, for a better predictive

capability of the thermospheric density and drag, which are important for satellite traffic control, it is critical that the impact of these storms be well understood.

Earlier investigations using thermospheric density measurements from LEO satellites have provided results on the density enhancement during geomagnetic storm events (e.g., Forbes et al., 1996; Sutton et al., 2005; Crowley et al., 2006). But the exact mechanisms through which the temperature and density perturbations distribute over the globe are still being investigated. It is not always true that the temperature and density enhancements occur at the exact location where the Joule heating occurs. In fact it has been observed that the temperature increase happens globally but larger enhancements occur at higher latitudes (Laskar, Eastes, et al., 2021). Moreover, as geomagnetic storm events change the thermospheric circulation, the largest enhancements occur mostly in regions where the horizontal motion of the air converges (Burns et al., 1995; Laskar, Eastes, et al., 2021).

The current capabilities of estimating the thermospheric neutral density and temperature using empirical models are generally good on the global average, but their estimation abilities are limited and they cannot forecast the spatial structures and conditions, particularly during a geomagnetic storm. However, the knowledge gained from currently available satellite based measurements can improve results from the empirical models. Also, incorporating the current observations in a whole atmosphere assimilation and forecasting system could potentially improve the current understanding of the TI system. Moreover, the altitudes lower than 200 km are below the reach of in-situ satellite measurements, and remote sensing of the altitudes between 120 and 250 km has been rare (Forbes et al., 1996). In this investigation we use data from NASA's Global-scale Observations of Limb and Disk (GOLD) mission to study a minor geomagnetic event and show that their use improves the thermospheric empirical model results, providing a better understanding of the storm time TI system (Laskar et al., 2022). A quantification of the thermospheric temperature changes in response to the storm has been made with GOLD data, which is then simulated in an empirical model to quantify the vertical profiles of the thermospheric density changes. The results are then compared with a state-of-the-art magnetosphere-ionosphere-thermosphere coupled model simulation.

2 Data, Model, and Methodology

GOLD disk temperature T_{disk} is compared with predictions from the Mass Spectrometer Incoherent Scatter- radar version 2 (MSIS2) and Multiscale Atmosphere Geospace Environment (MAGE) models. The MSIS2 is forced with different level of geomagnetic activity to simulate a GOLD T_{disk} equivalent run. The MAGE model is used to compare its densities with the GOLD informed MSIS2 calculations. Further details of these data and models are given below.

2.1 GOLD T_{disk}

GOLD observes the Earth's disk and limb in the FUV for over 18.5 hours each day, from 0610 to 0040 UT of the next day (Eastes et al., 2019, 2020; McClintock et al., 2020; Laskar et al., 2020). The daytime disk measurements cover about 0610 UT to 2300 UT. GOLD daytime disk scans of the N_2 Lyman-Birge-Hopfield (LBH) bands are used to retrieve the T_{disk} data. As the GOLD N_2 LBH emissions are column integrated quantities, the retrieved T_{disk} products are a representative of the corresponding N_2 LBH layer. The altitude of the layer has a range of 150 to 220 km which varies with solar zenith angle (SZA) and emission angle. But the peak altitudes remain below 200 km for SZA and emission angles less than 70° (Evans et al., 2018; Laskar, Pedatella, et al., 2021). GOLD scans each full disk in about 30 minutes. The T_{disk} retrieval algorithm is an improvement of the code that was used previously to derive temperature from limb measurements of N_2 LBH intensity from the High-resolution Ionospheric and Thermospheric Spectrograph (HITS) instrument (Aksnes et al., 2006; Krywonos et al., 2012; Evans et al., 2018). Effective neutral temperatures are retrieved by fitting the observed rotational structure of the N_2 LBH bands using an optimal estimation routine (Rodgers, 2000; Lumpe et al., 2002; Evans et al., 2018). The current investigation used Level 2 (L2) T_{disk} version 3 (V03) data that are retrieved from 2×2 binned level-1C N_2 LBH spectra, which are available at the GOLD web-page, `https://gold.cs.ucf.edu/` as 'Level 2—TDISK'. The 2×2 binned data have a spatial resolution of 250-km×250-km near nadir. Typical random errors in the 2×2 binned T_{disk} data varies with signal to noise ratio of the N_2 LBH emission and it ranges from 20 K (for high SNR) to 90 K (for low SNR).

2.2 NRLMSIS2.0 Model

Naval Research Laboratory (NRL) MSIS2.0 (NRLMSIS2.0) is an empirical model of the thermosphere. The earlier versions of MSIS (MSIS-86 and MSIS-90) simulated neutral composition, total mass density, and temperature (Hedin, 1987, 1991). MSIS-86 was available for altitudes above 90 km, whereas MSIS-90 was extend from the ground to the exobase (Hedin, 1991). Later development led to the NRLMSISE-00 which improved the total mass density by incorporating more orbital drag and accelerometer data (Picone et al., 2002). Recently, the model was further updated to NRLMSIS2.0 (Emmert et al., 2021). In this version, extensive new data were incorporated to estimate the profiles of neutral temperature, 8 neutral species densities, and total neutral mass density based on, time, location, solar activity, and geomagnetic activity. Emmert et al. (2021) noted relatively lower predicted temperature in this iteration of the model compared to its predecessor, which likely affects the neutral densities. NRLMSIS 2.0 densities are fully coupled to temperature from the ground to the exosphere via a hydrostatic/diffusive equilibrium profile. (see Emmert et al., 2021). We have used the latest iteration, NRLMSIS2.0, here onward we refer it as MSIS2.

2.3 MAGE Model

MAGE couples multiple models of the magnetosphere, the ring current, and the ionosphere-thermosphere into a coherent two-way coupling scheme. The model couples Grid Agnostic Magnetohydrodynamic model for Extended Research Applications (GAMERA) global model of magnetosphere (Sorathia et al., 2020), the Rice Convection Model of ring current (RCM; Toffoletto et al. (2003)), the Thermosphere-Ionosphere Electrodynamics General Circulation Model (TIEGCM; Qian et al. (2014); Richmond et al. (1992)), and the RE-developed Magnetosphere-Ionosphere Coupler/Solver (REMIX), which is a rewrite of the MIX code (Merkin & Lyon, 2010). Greater details of the coupling schemes and the working principle can be found in Lin et al. (2021) and Pham et al. (2022).

3 A Recent Geomagnetic Event and its Significance

On 3^{rd} February 2022 there was a geomagnetic storm, for which some of the geomagnetic parameters are shown in Figure 1. The storm started at about 00 UT on 3 February (as depicted by the vertical dashed-line) and was strengthen for a second time

near the universal time (UT) midnight of 4 February with an active phase lasting the whole day. The shaded region in Figure 1 represents the active days when IMF Bz (z component of Interplanetary Magnetic Field) was mostly southward, relatively faster solar wind, and two episodes of Dst index reaching down to -65 nT. Notably, on 3 February SpaceX launched 49 satellites to very low earth orbits (VLEO, about 210 km) in preparation to boost individual satellites into a higher operating orbit, of which 38 were lost due to an unusual increase in the satellite drag (Hapgood et al., 2022), which they reported to be about 50% higher compared to their previous experiences during low solar and quiet geomagnetic conditions. This event motivated us to investigate the thermospheric conditions using GOLD data and model simulations. This study is focused on characterizing the thermospheric conditions on these two days.

Based on the Dst index this storm could be classified as 'moderate' storm (Loewe & Prölss, 1997; Borovsky & Shprits, 2017). As Dst is not always a great indicator of geospace storm (McPherron & Chu, 2016; Borovsky & Shprits, 2017), we also use National Oceanic and Atmospheric Administration's (NOAA) Space Weather Prediction Center (SWPC) classification. The highest 3 hourly Kp and ap indices during this event were 5+ and 56 nT (Figure 1d), respectively as per NASA Omniweb (`https://omniweb.gsfc.nasa.gov/`). Based on the NOAA SWPC Space Weather Scales (`https://www.swpc.noaa.gov/sites/default/files/images/NOAAscales.pdf`) classification this storm is a minor (G1 class) event. So, we designate this as a 'minor' event.

4 Results

4.1 Results from GOLD Observations

Figure 2 shows the observations of the GOLD disk temperatures (T_{disk} in a-d) and difference from a quiet day (e-h) on 3 February 2022, when there was a minor geomagnetic storm. A 4x4 pixel (about a thousand km) smoothing of the temperature data are carried out to generate smooth looking images as presented in Figure 2. The background or baseline values are calculated by taking the average of the four days of T_{disk} data from 26 to 30 January 2022. The four days are chosen in such a way that the geomagnetic activity was quiet, so we excluded 29 Jan. 2022, which was a slightly disturbed day. Also, averaging the disks over four days reduces the day-to-day variability and the random noise, which varied from 20 to 90 K for a particular disk image, depending on the signal-to-

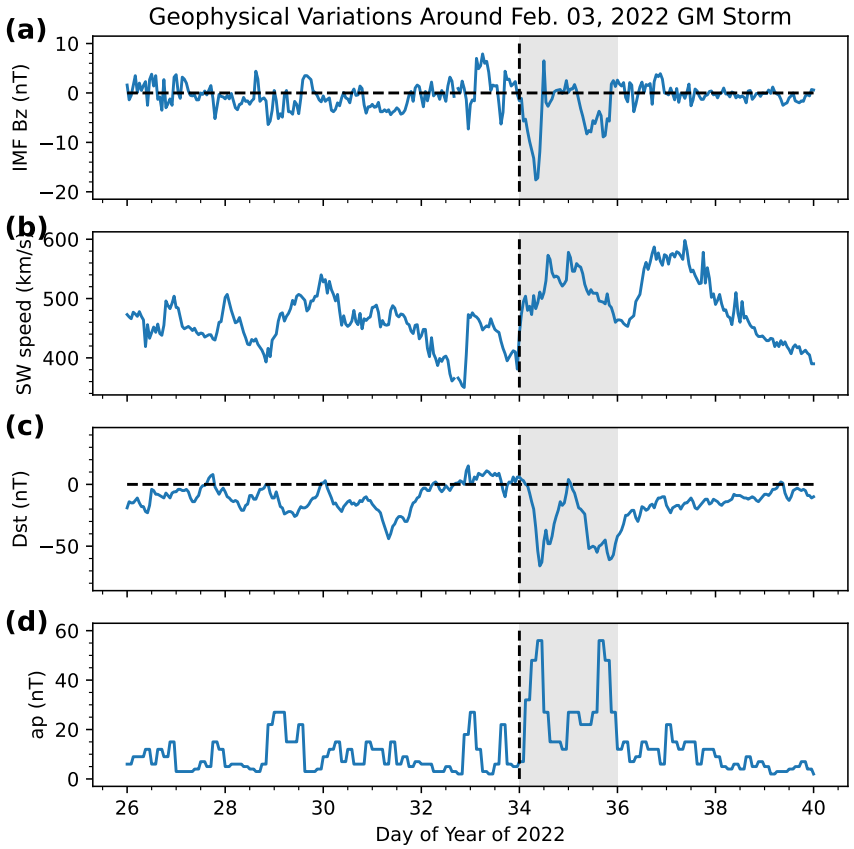

Figure 1. Geomagnetic indices and solar wind conditions in-and-around the 3^{rd} February 2022 minor geomagnetic storm. The shaded region represents the active days with IMF Bz mostly southward, relatively faster solar wind, and two episodes of Dst reaching below -50 nT.

noise ratio (SNR) of the LBH emissions measured at that location (Laskar et al., 2022). From the differences (ΔT) it can be noted that the values are positive over the majority of the disk on the storm day.

To investigate how the temperatures varied prior to, during, and after the geomagnetic storm, the day-to-day and latitudinal variations of the T_{disk} averaged over 40°W to 53°W longitude region and for UTs of the four full disk scans (that are shown in Figure 2) are shown in Figure 3 along with the solar F10.7 cm flux and 30 minute cadence geomagnetic ap index (Matzka et al., 2022; Yamazaki et al., 2022). Again, the temporal and spatial averaging is done to reduce the random noise in the GOLD T_{disk}. The temperature starts to increase from the day-of-year (DOY) 34, when there happened a geomagnetic storm starting very early in the morning of 3 February 2022 as can be seen from Figure 1 and from the ap index in Figure 3. We are not sure what caused the un-

usual increase at every latitude on Jan. 31, which needs further investigations. However, it can be stated it is not an effect of geomagnetic activity as that day was quiet. Also, temperature enhancement due to geomagnetic activity shows a characteristic feature of relatively larger enhancements at higher latitudes (Laskar, Eastes, et al., 2021), which is not clear in this particular day.

To calculate the average increase in temperature over the disk, UTs of the four full-disk scans of data as shown in Figure 2 are averaged for the two storm days (3 and 4 Feb.) and a similar averaging is done for the baseline quiet day (in this case 1 Feb. 2022). Considering the 1^{st} February as the baseline day, the temperature difference between active and quiet times is about 61 K, with errors below 1 K as the calculations are done with more than four thousand data points over the disk. Note that the ΔT values are subject to the reference day being selected but for all possible quiet days within 26 January to 2 February the values vary from 47 K (with 31 Jan. as baseline) to 95 K (with 26 Jan as baseline). Note that the 61 K increase in T_{disk} and the range of this increase (47 to 95 K, with respect to other baselines) are the primary findings from GOLD and they will be used later for estimations of thermospheric density perturbations at different altitudes.

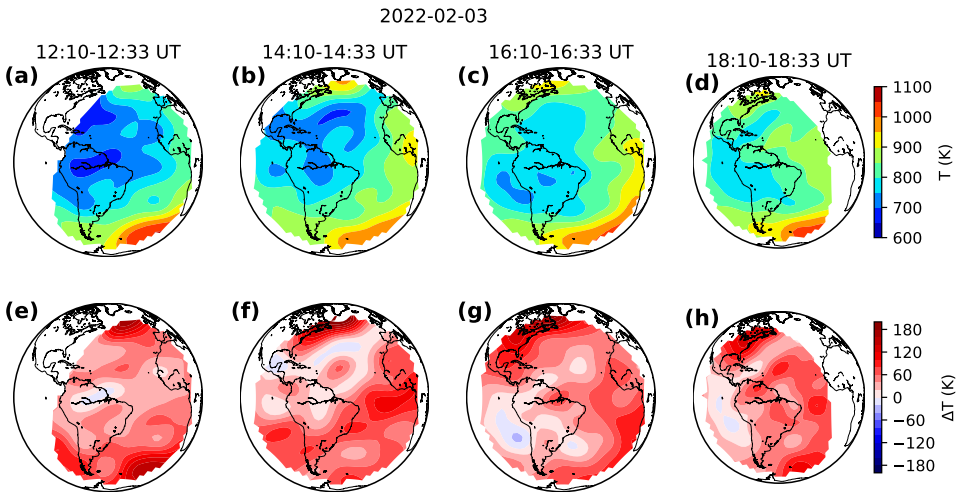

Figure 2. T_{disk} (referred to as T here, 'a' to 'd') and difference from quiet time (ΔT, 'e' to 'h') on 3^{rd} February 2022 are shown. The bottom panels show a mostly positive ΔT, suggesting an overall increase in the thermospheric temperature with respect to the pre-storm reference.

4.2 Results from Model Simulations

As presented above, we have made an estimate of the lower- and middle-thermospheric T_{disk} enhancement during the storm event. To estimate the corresponding thermospheric density changes in response to the geomagnetic storm, we have used two different simulation approaches. 1) an empirical method in which MSIS2 was used to simulate thermospheric conditions that are equivalent to GOLD temperature increase and 2) MAGE model simulations. The MAGE model is used for an independent comparison of the calculations made using MSIS2 assisted with knowledge gained from GOLD (here onward we refer this as MSIS-GOLD). As mentioned above, from GOLD we have observed a temperature increase of about 61 K when averaged over the GOLD field of view. This temperature enhancement can expand the thermosphere and give rise to density increase at a given altitude. To find out how much the thermospheric density will change in response to this T_{disk} increase MSIS2 simulations are carried out.

Before we estimate the density changes with MSIS2, let us see how the GOLD T_{disk} compare with MSIS2 and MAGE temperatures. GOLD equivalent temperatures (T_{eff}) are calculated from MSIS2 and MAGE using contribution functions as reported in Laskar, Pedatella, et al. (2021). Figure 4 shows the comparison plots for the four disk scans taken on the storm day, 3^{rd} February 2022. It can be seen that the MSIS2-T_{eff} is smaller than GOLD, and the MAGE-T_{eff} is in better agreement with GOLD T_{disk}. The percentage deviations of model temperatures with respect to T_{disk} are about 6.9% for MSIS2 and 2.3% for MAGE, which suggests that the thermospheric temperature are underestimated in both MSIS2 and MAGE.

Though MSIS2 underestimates the thermospheric temperature when compared with GOLD, the model can be used to investigate how much density change can happen in response to a change in T_{eff}. Therefore, we use MSIS2 to estimate the change in thermospheric neutral density in response to the 61 K increase observed in GOLD T_{disk}. Being an empirical model, MSIS2 can be forced with various geomagnetic conditions to see their impact on the thermospheric temperature and neutral density. So, we have used a set of geomagnetic ap indices ranging from 0 to 390 nT to find out what level of geomagnetic activity is needed to observe a T_{eff} difference that is the same as that observed from GOLD (61 K as mentioned above). Figure 5(a) shows the temperature difference between different MSIS2 runs with varied ap index. To calculate the perturba-

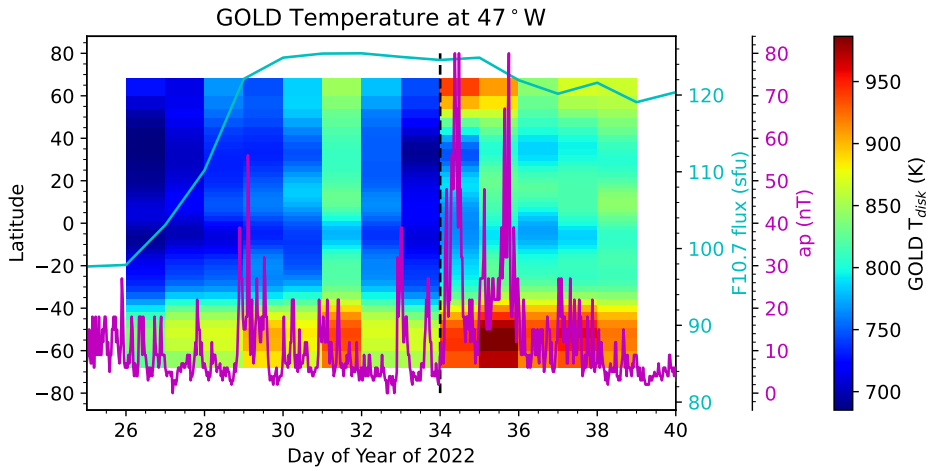

Figure 3. Day-to-day and latitudinal variability of the GOLD disk temperatures averaged between 40-53°W in and around the geomagnetic storm on 3 and 4 February 2022. An increase in temperature can be noted from day 34, when there was a geomagnetic storm as can be seen from the 30 minute cadence ap index values.

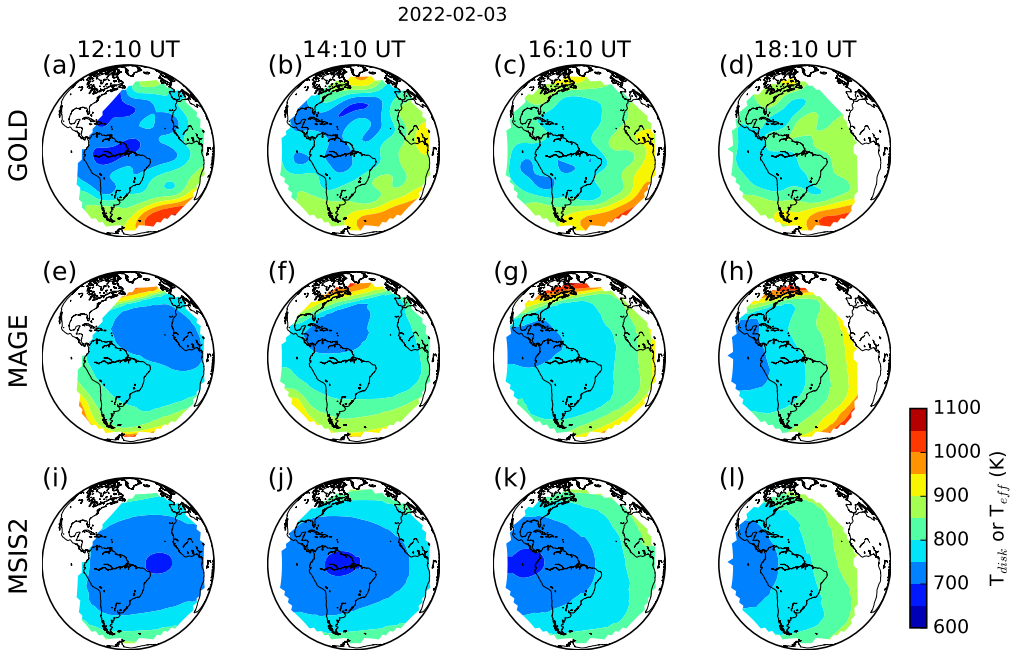

Figure 4. (a-d)GOLD T_{disk} for the four disk scans on the storm day, (e-f) GOLD equivalent effective temperature (T_{eff}) from the MAGE model, and (i-l) GOLD equivalent effective temperature (T_{eff}) from MSIS2. Notable features are that the GOLD and MAGE-T_{eff} are in good agreement but the MSIS2 underestimate the T_{eff}.

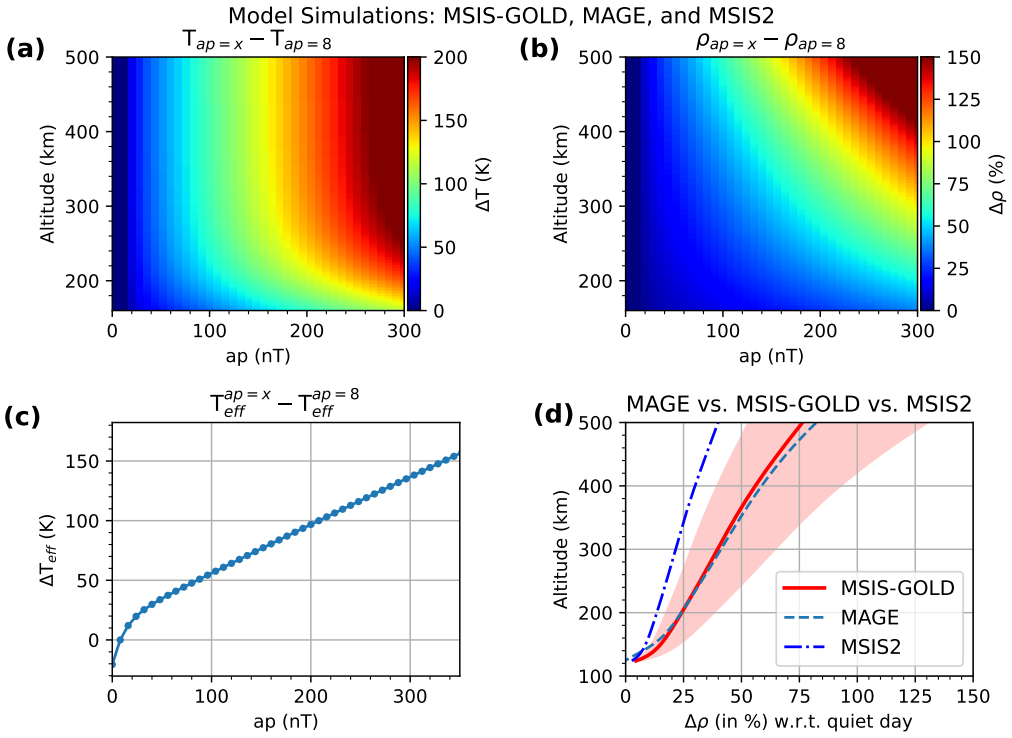

Figure 5. MSIS2 model simulation of thermospheric temperature difference (a) and percentage change in neutral density (b) in response to changing geomagnetic activity levels (varied ap indices). MSIS2 effective temperature differences (c) with respect to ap=8 level and the altitude variation of density for an ap level of 116 nT (d). The ap=116 nT corresponds to a ΔT_{eff} of 61 K. Panel (d) also shows the range of densities for ΔT_{eff} values between 47 K and 95 K. MAGE simulation and MSIS2 model simulated percentage density differences are also shown in (d).

tions MSIS2 simulation states corresponding to an ap value of 8 nT has been used as the baseline. This is because, an earlier study by Laskar, Eastes, et al. (2021) has shown that the base level of geomagnetic activity that does not perturb the thermospheric temperature is about 8 nT. Other input parameters, such as, universal time (UT), geo-location, F10.7 and F10.7A are set at 15 UT, 60°N to 60°S & 48°W, 100 sfu, and 100 sfu, respectively. Note 1 sfu=10^{-22}W m^{-2} Hz^{-1}. From the temperature differences (in Figure 5a), it can be seen clearly that with increasing geomagnetic activity the thermospheric temperatures increase, also the corresponding density differences (in Figure 5b) are positive and increasing with increasing geomagnetic activity level.

To further quantify the thermospheric conditions the effective temperatures averaged over 60°N to 60°S are shown in Figure 5(c) for the ap indices considered. From Figure 5(c) we can estimate that an ap index of 116 nT is needed, which is about 60 nT higher than the maximum 3 hourly ap value observed on that day, for MSIS2 to reproduce a T_{eff} difference of 61 K. We have also identified the MSIS2 simulations for which the effective temperature differences are 47 K (ap=82 nT) and 95 K (ap=202 nT). The neutral density enhancements for the simulations with ap=116 nT and those corresponding to T_{eff} differences of 47 K and 95 K are also shown in Figure 5(d). The region between density differences corresponding to T_{eff} differences of 47 K and 95 K are shown as shadowed region, as they represent a range of values based on various baseline levels. From this plot one can estimate that the neutral density increase in the thermosphere during the storm ranged from 15% at 150 km altitude to about 80% at 500 km. Also, the density difference at 210 km is about 25% and it can range from 15% to 45% based on which day is being selected as the reference. For a comparison purpose the density enhancement using only the MSIS2, with F10.7=120 sfu and 3 hour ap=56 nT for storm day and 8 nT for quiet day, is also shown in Figure 5(d). Note that the MSIS2 only calculation underestimated the density enhancement by 44% at 200 km compared to GOLD-MSIS, whereas the MAGE agree well with GOLD-MSIS. It may be noted that most of the prior SpaceX launches were into an F10.7<100 sfu environment, and many were F10.7<80 sfu. So the density increase relative to those earlier launches would be much larger than 15% (at 150 km).

In addition to the MSIS-GOLD estimated density changes, that are retrieved based on the T_{eff} difference of 61 K, the MAGE model calculation of thermospheric neutral density changes are also shown in Figure 5(d) with a dashed line. Similar to GOLD cal-

culations, 1^{st} February has been used as the baseline quiet day. Also, the temporal and spatial averaging of the densities are similar to GOLD. The MAGE model calculated $\Delta\rho$ (3^{rd} and $4^{th}$with reference to 1^{st}) is in good agreement with GOLD assisted MSIS2 (MSIS-GOLD) calculation. This comparison also validates MAGE simulation indicating that the coupled geospace MAGE model, which describes better the location and strength of Joule heating during a storm, as well as their temporal evolution (Pham et al., 2022), predicts temperature changes close to GOLD observations. These two independent calculations demonstrate that the thermospheric density increased significantly during the minor geomagnetic storm on February 3-4, 2022. Therefore, drag on the low-earth orbiting satellites would change proportionately, which could potentially be responsible for VLEO satellite deorbiting.

5 Discussion

The increased density at thermospheric altitudes has great implications on the satellite drag estimation. For a 15% increase in density it is necessary for a VLEO satellite to have sufficient thrust to overcome the drag and maintain the altitude. Even though, the current geomagnetic storm was a minor event it has impacted the density so much (about 25% at 200 km) that the corresponding drag could potentially be responsible for satellite deorbiting. If the storms are severe to extreme, they would increase the density enormously and therefore the loss could be severe. Therefore, it is necessary to update the current empirical and forecasting models with state-of-the-art experimental measurements for a better forecast capability of the thermospheric densities, particularly at LEO altitudes. These results also indicate that GOLD T_{disk} observations can be assimilated in data assimilation and forecasting models to improve the nowcasts and forecasts. Also, the GOLD data can be used to improve the empirical models, e.g., MSIS2. As the impact of geomagnetic storms varies with latitude, an elliptic satellite with a perigee at high-latitude will have different drag compared to a low-latitude perigee. Also, for such orbits the knowledge of drag at perigee altitudes is critical as most of the interplanetary missions are launched in this configuration, which increase their apogee based on thrust at the altitude of perigee. So, avoiding low altitude perigee is best to be safe from effects of space weather related impacts.

6 Summary and Conclusions

Thermospheric conditions during the minor geomagnetic storm on 3^{rd} and 4^{th} February 2022 are investigated using GOLD disk temperature measurements and simulations using MSIS2 and MAGE. The salient results are summarized below:

1. GOLD T_{disk} was about 61 K higher for the storm days compared to a pre-storm quiet time.
2. MSIS simulation corresponding to the 61 K T_{eff} enhancement shows about 15% (at 150 km) to 80% (at 500 km) density increase.
3. T_{eff} simulated by MAGE are about 2% lower than GOLD T_{disk}. For MSIS2 it is about 7% lower.
4. Neutral density enhancement in response to a minor storm in MAGE agrees well with GOLD assisted MSIS density simulations.

These results show that the even during a minor geomagnetic storm the thermospheric density and therefore the drag can be perturbed significantly. Also, it shows that the current empirical models (e.g., MSIS2) underestimate the density enhancement in response to minor events. This also demonstrates that there is a great potential of the GOLD T_{disk} to improve thermospheric density forecast models.

Acknowledgments

This research was supported by NASA Contract 80GSFC18C0061 to the University of Colorado, Boulder. This material is also based upon work supported by the National Center for Atmospheric Research (NCAR), which is a major facility sponsored by the National Science Foundation under Cooperative Agreement No. 1852977. This work was also supported in part by NASA HSR grants 80NSSC19K0835, 80NSSC20K0356, and 80NSSC20K0601. DL was supported by NASA GCR grant 80NSSC17K0013, DRIVE Science Center for Geospace Storms (CGS) under grant 80NSSC20K0601, LWS grant 80NSSC21K0008, and HSR grant 80NSSC21K1677. The Level 2 data used in this study are available at the GOLD Science Data Center (`https://gold.cs.ucf.edu/search/`) and at NASA's Space Physics Data Facility (`https://spdf.gsfc.nasa.gov/pub/data/gold/level2/tdisk/`). The derived data products from MAGE are available at `https://doi.org/10.5281/zenodo.6807766`. The ap index and F10.7 flux data are obtained from NASA omniweb (`https://omniweb.gsfc.nasa.gov/`).

References

Aa, E., Zhang, S.-R., Erickson, P. J., Coster, A. J., Goncharenko, L. P., Varney, R. H., & Eastes, R. (2021, jul). Salient midlatitude ionosphere-thermosphere disturbances associated with SAPS during a minor but geo-effective storm at deep solar minimum. *Journal of Geophysical Research: Space Physics*, *126*(7). doi: 10.1029/2021ja029509

Aksnes, A., Eastes, R., Budzien, S., & Dymond, K. (2006). Neutral temperatures in the lower thermosphere from N_2 Lyman-Birge-Hopfield (LBH) band profiles. *Geophysical Research Letters*, *33*(15). doi: 10.1029/2006gl026255

Borovsky, J. E., & Shprits, Y. Y. (2017, nov). Is the dst index sufficient to define all geospace storms? *Journal of Geophysical Research: Space Physics*, *122*(11). doi: 10.1002/2017ja024679

Bruinsma, S., Forbes, J. M., Nerem, R. S., & Zhang, X. (2006). Thermosphere density response to the 20–21 november 2003 solar and geomagnetic storm from CHAMP and GRACE accelerometer data. *Journal of Geophysical Research*, *111*(A6). doi: 10.1029/2005ja011284

Burns, A. G., Killeen, T. L., Deng, W., Carignan, G. R., & Roble, R. G. (1995). Geomagnetic storm effects in the low- to middle-latitude upper thermosphere. *Journal of Geophysical Research*, *100*(A8), 14673. doi: 10.1029/94ja03232

Cai, X., Burns, A. G., Wang, W., Qian, L., Pedatella, N., Coster, A., ... McClintock, W. E. (2021, June). Variations in thermosphere composition and ionosphere total electron content under "geomagnetically quiet" conditions at solar-minimum. *Geophysical Research Letters*, *48*(11). doi: 10.1029/2021gl093300

Cai, X., Burns, A. G., Wang, W., Qian, L., Solomon, S. C., Eastes, R. W., ... Laskar, F. I. (2021, June). Investigation of a neutral "tongue" observed by GOLD during the geomagnetic storm on may 11, 2019. *Journal of Geophysical Research: Space Physics*, *126*(6). doi: 10.1029/2020ja028817

Crowley, G., Hackert, C. L., Meier, R. R., Strickland, D. J., Paxton, L. J., Pi, X., ... Wene, G. (2006, October). Global thermosphere-ionosphere response to onset of 20 november 2003 magnetic storm. *Journal of Geophysical Research*, *111*(A10). Retrieved from `https://doi.org/10.1029/2005ja011518` doi: 10.1029/2005ja011518

Eastes, R. W., McClintock, W. E., Burns, A. G., Anderson, D. N., Andersson, L., Aryal, S., ... Woods, T. N. (2020, June). Initial observations by the GOLD mission. *Journal of Geophysical Research: Space Physics*, *125*(7). doi: 10.1029/2020ja027823

Eastes, R. W., Solomon, S. C., Daniell, R. E., Anderson, D. N., Burns, A. G., England, S. L., ... McClintock, W. E. (2019, August). Global-scale observations of the equatorial ionization anomaly. *Geophysical Research Letters*, *46*(16), 9318–9326. doi: 10.1029/2019gl084199

Emmert, J. T., Drob, D. P., Picone, J. M., Siskind, D. E., Jones, M., Mlynczak, M. G., ... Yuan, T. (2021, mar). NRLMSIS 2.0: A whole-atmosphere empirical model of temperature and neutral species densities. *Earth and Space Science*, *8*(3). doi: 10.1029/2020ea001321

Evans, J. S., Eastes, R., Lumpe, J. D., Correira, J., Burns, A. G., McClintock, B., ... Veibell, V. (2018, December). Global-scale Observations of the Limb and Disk (GOLD): Overview of Daytime Neutral Temperature Science Data Product. In *Agu fall meeting abstracts* (Vol. 2018, p. SA21A-3172).

Forbes, J. M., Gonzalez, R., Marcos, F. A., Revelle, D., & Parish, H. (1996, feb). Magnetic storm response of lower thermosphere density. *Journal of Geophysical Research: Space Physics*, *101*(A2), 2313–2319. doi: 10.1029/95ja02721

Fuller-Rowell, T. J., Codrescu, M. V., Moffett, R. J., & Quegan, S. (1994). Response of the thermosphere and ionosphere to geomagnetic storms. *Journal of Geophysical Research*, *99*(A3), 3893. doi: 10.1029/93ja02015

Hapgood, M., Liu, H., & Lugaz, N. (2022, mar). SpaceX—sailing close to the space weather? *Space Weather*, *20*(3). doi: 10.1029/2022sw003074

Hedin, A. E. (1987). MSIS-86 thermospheric model. *Journal of Geophysical Research*, *92*(A5), 4649. doi: 10.1029/ja092ia05p04649

Hedin, A. E. (1991, feb). Extension of the MSIS thermosphere model into the middle and lower atmosphere. *Journal of Geophysical Research: Space Physics*, *96*(A2), 1159–1172. doi: 10.1029/90ja02125

Krywonos, A., Murray, D. J., Eastes, R. W., Aksnes, A., Budzien, S. A., & Daniell, R. E. (2012, September). Remote sensing of neutral temperatures in the Earth's thermosphere using the Lyman-Birge-Hopfield bands of N_2: Comparisons with satellite drag data. *Journal of Geophysical Research: Space Physics*,

117(A9). doi: 10.1029/2011ja017226

Laskar, F. I., Eastes, R. W., Codrescu, M. V., Evans, J. S., Burns, A. G., Wang, W., ... Cai, X. (2021, aug). Response of GOLD retrieved thermospheric temperatures to geomagnetic activities of varying magnitudes. *Geophysical Research Letters*, *48*(15). doi: 10.1029/2021gl093905

Laskar, F. I., Eastes, R. W., Martinis, C. R., Daniell, R. E., Pedatella, N. M., Burns, A. G., ... Codrescu, M. V. (2020, July). Early morning equatorial ionization anomaly from GOLD observations. *Journal of Geophysical Research: Space Physics*, *125*(7). doi: 10.1029/2019ja027487

Laskar, F. I., Pedatella, N. M., Codrescu, M. V., Eastes, R. W., Evans, J. S., Burns, A. G., & McClintock, W. (2021, January). Impact of GOLD retrieved thermospheric temperatures on a whole atmosphere data assimilation model. *Journal of Geophysical Research: Space Physics*, *126*(1). doi: 10.1029/2020ja028646

Laskar, F. I., Pedatella, N. M., Codrescu, M. V., Eastes, R. W., & McClintock, W. E. (2022, mar). Improving the thermosphere ionosphere in a whole atmosphere model by assimilating GOLD disk temperatures. *Journal of Geophysical Research: Space Physics*, *127*(3). doi: 10.1029/2021ja030045

Li, R., & Lei, J. (2021, jan). Responses of thermospheric mass densities to the october 2016 and september 2017 geomagnetic storms revealed from multiple satellite observations. *Journal of Geophysical Research: Space Physics*, *126*(1). doi: 10.1029/2020ja028534

Lin, D., Sorathia, K., Wang, W., Merkin, V., Bao, S., Pham, K., ... Anderson, B. (2021, dec). The role of diffuse electron precipitation in the formation of subauroral polarization streams. *Journal of Geophysical Research: Space Physics*, *126*(12). doi: 10.1029/2021ja029792

Liu, H., & Lühr, H. (2005, August). Strong disturbance of the upper thermospheric density due to magnetic storms: CHAMP observations. *Journal of Geophysical Research: Space Physics*, *110*(A9). doi: 10.1029/2004ja010908

Liu, R., Lühr, H., & Ma, S.-Y. (2010, jan). Storm-time related mass density anomalies in the polar cap as observed by CHAMP. *Annales Geophysicae*, *28*(1), 165–180. doi: 10.5194/angeo-28-165-2010

Loewe, C. A., & Prölss, G. W. (1997, jan). Classification and mean behavior of magnetic storms. *Journal of Geophysical Research: Space Physics*, *102*(A7),

14209–14213. doi: 10.1029/96ja04020

Lumpe, J. D., Bevilacqua, R. M., Hoppel, K. W., & Randall, C. E. (2002, November). POAM III retrieval algorithm and error analysis. *Journal of Geophysical Research: Atmospheres*, *107*(D21), ACH 5–1–ACH 5–32. Retrieved from `https://doi.org/10.1029/2002jd002137` doi: 10.1029/2002jd002137

Matzka, J., Bronkalla, O., Kervalishvili, G., Rauberg, J., & Yamazaki, Y. (2022). *Geomagnetic hpo index.* GFZ Data Services. Retrieved from `https://www.gfz-potsdam.de/hpo-index/` doi: 10.5880/HPO.0002

McClintock, W. E., Eastes, R. W., Beland, S., Bryant, K. B., Burns, A. G., Correira, J., ... Veibel, V. (2020, May). Global-scale observations of the limb and disk mission implementation: 2. observations, data pipeline, and level 1 data products. *Journal of Geophysical Research: Space Physics*, *125*(5). doi: 10.1029/2020ja027809

McPherron, R. L., & Chu, X. (2016, nov). The mid-latitude positive bay and the MPB index of substorm activity. *Space Science Reviews*, *206*(1-4), 91–122. doi: 10.1007/s11214-016-0316-6

Merkin, V. G., & Lyon, J. G. (2010, oct). Effects of the low-latitude ionospheric boundary condition on the global magnetosphere. *Journal of Geophysical Research: Space Physics*, *115*(A10), n/a–n/a. doi: 10.1029/2010ja015461

Pham, K. H., Zhang, B., Sorathia, K., Dang, T., Wang, W., Merkin, V., ... Lyon, J. (2022, feb). Thermospheric density perturbations produced by traveling atmospheric disturbances during august 2005 storm. *Journal of Geophysical Research: Space Physics*, *127*(2). doi: 10.1029/2021ja030071

Picone, J. M., Hedin, A. E., Drob, D. P., & Aikin, A. C. (2002, dec). NRLMSISE-00 empirical model of the atmosphere: Statistical comparisons and scientific issues. *Journal of Geophysical Research: Space Physics*, *107*(A12), SIA 15–1–SIA 15–16. doi: 10.1029/2002ja009430

Prölss, G. W. (2010, dec). Density perturbations in the upper atmosphere caused by the dissipation of solar wind energy. *Surveys in Geophysics*, *32*(2), 101–195. doi: 10.1007/s10712-010-9104-0

Qian, L., Burns, A. G., Emery, B. A., Foster, B., Lu, G., Maute, A., ... Wang, W. (2014, mar). The NCAR TIE-GCM. In *Modeling the ionosphere-thermosphere system* (pp. 73–83). John Wiley & Sons, Ltd. doi: 10.1002/

9781118704417.ch7

Richmond, A. D. (2021). Joule heating in the thermosphere. In *Upper atmosphere dynamics and energetics* (p. 1-18). American Geophysical Union (AGU). doi: 10.1002/9781119815631.ch1

Richmond, A. D., Ridley, E. C., & Roble, R. G. (1992, mar). A thermosphere/ionosphere general circulation model with coupled electrodynamics. *Geophysical Research Letters*, *19*(6), 601–604. doi: 10.1029/92gl00401

Rodgers, C. D. (2000). *Inverse methods for atmospheric sounding.* WORLD SCIENTIFIC. doi: 10.1142/3171

Sorathia, K. A., Merkin, V. G., Panov, E. V., Zhang, B., Lyon, J. G., Garretson, J., ... Wiltberger, M. (2020, jul). Ballooning-interchange instability in the near-earth plasma sheet and auroral beads: Global magnetospheric modeling at the limit of the MHD approximation. *Geophysical Research Letters*, *47*(14). Retrieved from `https://doi.org/10.1029%2F2020gl088227` doi: 10.1029/2020gl088227

Sutton, E. K., Forbes, J. M., & Nerem, R. S. (2005, sep). Global thermospheric neutral density and wind response to the severe 2003 geomagnetic storms from CHAMP accelerometer data. *Journal of Geophysical Research: Space Physics*, *110*(A9). doi: 10.1029/2004ja010985

Toffoletto, F., Sazykin, S., Spiro, R., & Wolf, R. (2003). Inner magnetospheric modeling with the rice convection model. *Space Science Reviews*, *107*(1/2), 175–196. doi: 10.1023/a:1025532008047

Yamazaki, Y., Matzka, J., Stolle, C., Kervalishvili, G., Rauberg, J., Bronkalla, O., ... Jackson, D. R. (2022, may). Geomagnetic activity index hpo. *Geophysical Research Letters*, *49*(10). doi: 10.1029/2022gl098860

Yuan, L., Jin, S., & Calabia, A. (2019, mar). Distinct thermospheric mass density variations following the september 2017 geomagnetic storm from GRACE and swarm. *Journal of Atmospheric and Solar-Terrestrial Physics*, *184*, 30–36. doi: 10.1016/j.jastp.2019.01.007